CrystEngComm

PAPER

View Article Online
View Journal | View Issue

Cite this: *CrystEngComm*, 2025, **27**, 6155

n → π* and chalcogen bonds in azole-substituted isoindole derivatives: a combined crystallographic and computational study

Irina A. Kolesnik,[a] Vladimir I. Potkin,[a] Mikhail S. Grigoriev,[b] Rosa M. Gomila,[c] Eugeniya V. Nikitina,[d] Vladimir P. Zaytsev,[d] Fedor I. Zubkov *[d] and Antonio Frontera *[c]

A straightforward and efficient protocol for the synthesis of azole-substituted 3*a*,6-epoxyisoindolone-7-carboxylic acid derivatives is reported. The series comprises esters and an amide featuring isoxazole, thiazole, and isothiazole fragments. All compounds were comprehensively characterized by spectroscopic techniques and single-crystal X-ray diffraction. Detailed solid-state analysis, supported by DFT calculations, reveals the interplay of several noncovalent interactions, including lone pair–π* (n → π*), hydrogen bonding (HB), and chalcogen bonding (ChB). Non-covalent interaction (NCI) plot and natural bond orbital (NBO) analyses show that ester derivatives preferentially engage in n → π* interactions, while both thiazole-containing compounds exhibit more pronounced intramolecular ChBs, with sulfur atoms acting as σ-hole donors. Electron localization function (ELF) analysis further confirms the directional nature of these interactions. While various noncovalent interactions contribute to crystal packing, our study focuses specifically on the interplay of n → π*, hydrogen bonding, and chalcogen bonding. The combination of crystallographic and computational analyses provides new insights into how these less conventional forces cooperatively govern molecular conformation and solid-state assembly. Moreover, the calculated stabilization energies enable a comparative assessment of the relative strengths of n → π*, HB, and ChB contacts within this series.

Received 4th July 2025,
Accepted 5th August 2025

DOI: 10.1039/d5ce00673b

rsc.li/crystengcomm

Introduction

Pyrrolidine and its condensed derivatives hold an important position in medicinal chemistry due to their crucial role in a wide array of natural and synthetic compounds exhibiting antiviral, antibacterial, antifungal, antitumor, and various other biological activities.[1] Among the fused pyrrolidines, the dihydro(iso)indole, oxoindole, and oxoisoindole cores serve as foundational motifs for numerous well-known pharmacologically active alkaloids and medicinal substances.[2] Consequently, these heterocycles remain a significant focus of synthetic organic chemistry.

Additionally, azoles are highly important among bioactive heterocycles. For example, isoxazole serves as a key structural element in various important pharmaceuticals, including the antibiotics sulfamethoxazole and sulfisoxazole, the antidepressant isocarboxazid, the anti-rheumatic drug leflunomide, the nonsteroidal anti-inflammatory drug valdecoxib, and the antitumor agent danazol. Many compounds with anti-inflammatory, analgesic, antipyretic, anti-tuberculosis, antimicrobial, antifungal, and anticancer properties also feature an isoxazole core.[3] The isothiazole ring is a part of the structure of the microbicide sulfamethizole, and neuroleptics like ziprasidone and perospirone, as well as compounds demonstrating anti-poliovirus activity, with additional therapeutic potential in treating Parkinson's disease, diabetes, and cancer.[4] One particularly noteworthy feature of azoles is their ability to enhance the efficacy of conventional antitumor agents.[5]

The combination of azole and pyrrolidine moieties within a single molecule holds significant promise for the development of new multitarget medications. This necessity arises from the growing resistance of pathogens to existing drugs and the complex nature of many diseases.

[a] *Institute of Physical Organic Chemistry of National Academy of Sciences of Belarus, 13 Surganov str., 220072 Minsk, Belarus. E-mail: irynakolesnik93@gmail.com*
[b] *Frumkin Institute of Physical Chemistry and Electrochemistry, Russian Academy of Sciences, 31 Bldg 4, Leninsky prosp., Moscow, 119071, Russian Federation. E-mail: mickgrig@mail.ru*
[c] *Department of Chemistry, Universidad de les Islas Baleares, Crta. de Valldemosa km 7.5, 07122 Palma de Mallorca, Baleares, Spain. E-mail: toni.frontera@uib.es*
[d] *Faculty of Science, RUDN University, 6 Miklukho-Maklaya St., 117198 Moscow, Russian Federation. E-mail: fzubkov1973@gmail.com*

The solid-state molecular assembly depends fundamentally on noncovalent interactions which enable rational crystal engineering.[6] The n → π* interaction which involves the orbital overlap of a lone pair (n) from a donor atom like oxygen with the antibonding π* orbital of an adjacent carbonyl group has been increasingly acknowledged as a significant yet subtle stabilizing force.[7] The molecular interaction displays a short contact distance and optimal Bürgi–Dunitz angle[8] leading to modest molecular stability enhancement while significantly affecting molecular conformation and packing.[9] Crystallographic and gas-phase spectroscopic studies show that in molecules like *N*-acyl homoserine lactones[10] and aspirin analogues,[11] respectively, n → π* interactions determine the molecular shape by forcing particular conformations and stabilizing folded structures while modifying reactivity through changes in electron density at the carbonyl acceptor. Even though n → π* interactions have been studied mainly in biological macromolecules and solution-phase chemistry their application in crystal-based supramolecular assemblies is now gaining significant attention.[12]

In this study, we present a convenient protocol for synthesizing azole derivatives of 2-substituted 3*a*,6-epoxyisoindolone-7-carboxylic acids **1–4**, illustrated in Scheme 1. These target compounds present a rigid core where the C-atom of the ester or amido group is located at four bond distance from the oxo O-atom of the core (1-oxo-tetrahydro-3*a*,6-epoxyisoindole fragment). This is therefore ideal to analyze n → π* interactions, as detailed in Scheme 2. Moreover, the different substitution at the N-atom of the 1-oxo-tetrahydro-3*a*,6-epoxyisoindole moiety allows analysis of the influence of H-bonding or chalcogen bonding on the n → π* interaction. Such interplay between the interactions and the different behaviour of the ester and amido groups has been analyzed using DFT calculations in the solid state (with periodic boundary conditions) and several computational tools like NCIplot and NBO analyses. Although a variety of noncovalent interactions influence crystal growth and packing of compounds **1–4**, our research is designed to specifically investigate the less common n → π* and chalcogen bonding interactions. The combination of azole and pyrrolidine moieties in this new class of compounds provides an ideal framework to analyze how these specific forces govern molecular conformation.

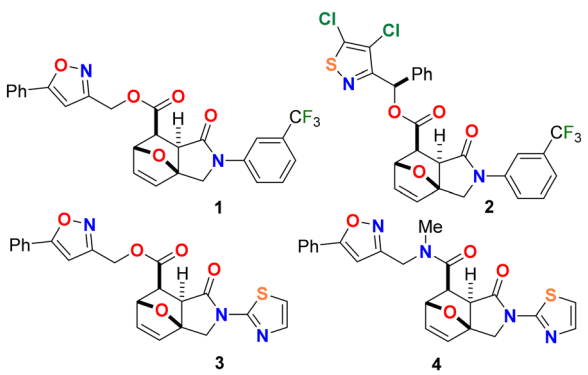

Scheme 1 Structures of compounds **1–4** reported in this work.

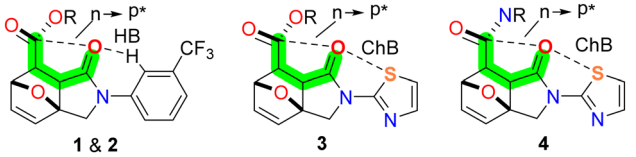

Scheme 2 Combination of n → π* and HB (**1** & **2**) or ChB (**3** & **4**) analyzed in this work.

Methods

Characterization of the target compounds

The synthesis of 3*a*,6-epoxyisoindolone derivatives **1–4** was performed according to a known procedure widely used for the preparation of carboxylic acid esters and amides.[13] 2-[3-(Trifluoromethyl)phenyl]- (**5a**) and 2-(thiazol-2-yl)- (**5b**) epoxyisoindole-7-carboxylic acids[14] as well as (5-phenylisoxazol-3-yl)methanol (**6a**),[15] (4,5-dichloroisothiazol-3-yl)(phenyl)methanol (**6b**)[16] and *N*-methyl-1-(5-phenylisoxazol-3-yl)methanamine (**6c**)[17] were used as starting materials (for synthesis and structures, see SI). Single crystals of compounds **1–4** for XRD analysis were obtained by slow evaporation of their saturated solutions in CH_2Cl_2 (**1**) or methanol (**2–4**). In addition to XRD, all obtained compounds were characterized using standard LCMS, FTIR and NMR spectroscopy (see SI).

In the ^{1}H NMR spectra of molecules **1**, **3**, and **4**, the exocyclic methylene groups appear as pairs of doublets in the range of δ 4.15–4.73 ppm with ^2J = 11.3–12.7 Hz; protons of the bicyclic fragment at tertiary carbon atoms are registered at δ 2.91–3.07, 3.00–3.41 and 5.11–5.31 ppm with J = 8.9–9.2 and 1.2–1.7 Hz. Protons at the multiple carbon–carbon bonds of the isoindole fragment are found at δ 6.50–6.69 ppm as doublets (J = 5.6–5.8 Hz) or a doublet of doublets (the second constant is J = 1.2–1.7 Hz). The thiazole protons in compounds **3** and **4** appear as doublets at δ 7.0–7.6 ppm; isoxazole protons (for **1**, **3** and **4**) are registered as a singlet at δ 6.7–7.0 ppm. In the ^{13}C NMR spectrum, the most noticeable signals of the C═O groups appear at δ 170.0–171.6 ppm and the signals of the thiazole ring are at δ 137.5–138.6 ppm (for **3** and **4**). In substances **1**, **3** and **4**, the tertiary C atom of the isoxazole ring is registered at δ 100–101 ppm. The carbon of the methylene bridge adjacent to the isoxazole appears at $\delta \sim$ 58.5 ppm in the case of esters and is shifted upfield in the case of the amide **4** (49.8 ppm).

The amide **4** in DMSO solution exists as a mixture of two rotamers **4-*E*/4-*Z*** (~75 : 25 at 25 °C), which is reflected in the doubling of the signals of protons and carbon atoms in ^{1}H and ^{13}C NMR spectra. This is connected with the inhibited rotation around the C–N bond due to the conjugation of the C═O bond π-electrons and the lone electron pair of the nitrogen atom. As a result, the amide exists in the form of *E*/

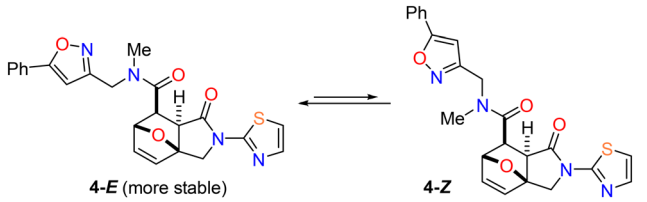

Scheme 3 Conformers of compound 4.

Z conformers that differ in stability (Scheme 3).[18] Despite this phenomenon manifested in solution, crystallization occurs in the form of the most stable (*E*)-conformer, which is confirmed by XRD analysis.

It is noteworthy that ester **2** was obtained as two diastereomers based on the orientation of the phenyl substituent. The ratio of these isomers was approximately 44 : 56; however, only one of them (the minor isomer) was isolated in pure form through fractional crystallization (for the structure, refer to Scheme 1). Probably, the major isomer turns out to be more soluble in methanol, so the minor one was eventually isolated in pure form. Isolation of the major diastereomer proved to be a challenging task due to the similar chromatographic behavior of both products.

X-ray analysis

X-Ray diffraction experiments were carried out on an automatic four-circle area-detector diffractometer Bruker KAPPA APEX II (MoKα radiation). The unit cell constants were refined over the whole data set together with data reduction.[19] The experimental intensities were corrected for absorption using the SADABS program.[20] The structures were solved by the intrinsic phasing method (SHELXT)[21] and refined by the full-matrix least-squares method (SHELXL-2018/3)[22] on F^2 for all data in the anisotropic approximation for all non-hydrogen atoms. The H atoms were placed in geometrically calculated positions with $U_{iso}(H) = 1.2U_{equ}(C)$.

The main crystallographic data and characteristics of X-ray diffraction experiment are given in Table S1. The atomic coordinates have been deposited with the Cambridge Crystallographic Data Centre, deposition numbers CCDC 2413571–2413574.

Theoretical methods

All periodic density functional theory (DFT) calculations were carried out using the TURBOMOLE 7.8 program package with periodic boundary conditions. Geometry optimizations were performed at the BP86 level of theory, combining the Becke 1988 exchange functional[23] with the Perdew 1986 correlation functional.[24] The pob-TZVP basis set[25] was employed for all atoms, along with the jbas universal fitting basis[25] for resolution-of-the-identity (RI) approximations.[26] Grimme's D3BJ dispersion correction[27] was included to account for long-range interactions. Single-point energy calculations were performed at the PBE0-D4/def2-TZVP level of theory[28,29] on the optimized geometries. These were used for further electronic structure analyses.

Noncovalent interaction (NCI) analysis was carried out using the Multiwfn program (version 3.8),[30] and the resulting reduced density gradient (RDG) isosurfaces were visualized with VMD.[31] Natural bond orbital (NBO) analysis was conducted using NBO 7.0 to assess donor–acceptor interactions and electronic delocalization effects.[32] Electron localization function (ELF) analysis[33] was also performed at the PBE0-D4/def2-TZVP level of theory using the Multiwfn program[30] to visualize σ-holes and lone pairs, providing insight into the directional nature of the interactions.

Results and discussion

Synthesis

Since the isoxazole and isothiazole derivatives of 1-oxo-epoxyisoindole-7-carboxylic acids have not been previously described, we began our research with the preparation of the simplest and most accessible compounds. As discussed earlier, the preparation of esters and an amide (**1–4**) was performed using the Steglich carbodiimide-mediated procedure, as outlined in 2021 by Jordan *et al.*[34] This method, which was originally developed for the synthesis of esters, allows for esterification and amidation under mild conditions. This enables the use of starting materials that are sensitive or insufficiently reactive for traditional protocols.[13] The inaccessibility of epoxyisoindole carboxylic acid chlorides was a key factor in selecting this synthetic approach. For our synthesis, we chose two available epoxyisoindole-7-carboxylic acids with trifluoromethylphenyl (**5a**) and thiazole (**5b**) substituents, as well as isoxazole-containing alcohol (**6a**), isothiazole-containing alcohol (**6b**), and an amine (**6c**) as starting materials (Scheme 4).

Esters **1–3** and amide **4** were synthesized by reacting the corresponding acids with heterocyclic alcohols or an amine in the presence of *N*,*N*′-dicyclohexylcarbodiimide (DCC) and *N*,*N*-dimethylaminopyridine (DMAP) as an acyl transfer

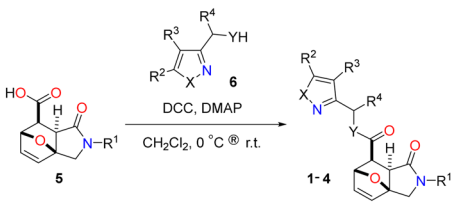

Initial compounds	Product	X	Y	R¹	R²	R³	R⁴	Yield, %
5a/6a	1	O	O		Ph	H	H	76
5a/6b	2	S	O		Cl	Cl	Ph	63
5b/6a	3	O	O		Ph	H	H	52
5b/6c	4	O	NMe		Ph	H	H	46

Scheme 4 Synthesis of esters **1–3** and amide **4**.

reagent (Scheme 4). Dichloromethane, which is commonly used in such reactions, was found to be suitable in this case due to its compatibility with the solubility of both the starting and final compounds.

Description of the structures

Compounds **1** and **2** contain intramolecular H-bonds of the C–H···O type (Fig. 1, S1 and S2, Tables S4 and S8, see the SI) between the amide oxygen (O1) and a proton of the $CF_3C_6H_4$ moiety. Interestingly, the most acidic hydrogen atom H12 takes part in this intramolecular interaction in **2**, whereas the H16 in the *para*-position towards the fluorine atom forms these bonds in **1**. This is explained by steric interactions between the trifluoromethyl group and the bulky, planar phenylisoxazole fragment, which causes both fragments to be located at the maximum distance from each other within the crystal structure of **1**. In contrast, the less bulky phenyl (isothiazole) substituent in the molecule **2** allows the trifluoromethyl group to occupy a *syn*-periplanar rearrangement relative to the N–C═O amide fragment. The torsion angle values are −16.1° for the molecule **1** (∠C1N2C11C16) and 2.1° in **2** (∠C1N2C11C12).

The amide moieties (∠C1N2C32S31) in **3** and **4** are almost flat: −11.0° for **3** and 0.3° for **4**. This predetermines the emergence of intramolecular n → π* contacts between sulfur (S31) and oxygen (O1) atoms.

For **1** and **2**, the O1···C8 distances are the same: 2.954 and 2.955 Å, while in structures **3** and **4**, the corresponding distances are slightly larger: 3.047 and 3.069 Å. The O1–C8–S31 angles (in structures **3** and **4**) and the corresponding O1–C8–H12(H16) angles (in structures **1** and **2**) range from 135.3° to 147.7°.

In the structure of **1**, a π–π interaction between parallel (around inversion center) isoxazole rings is present (Fig. S1). The distance between the centers of the rings is 3.428 Å, the shift is 0.612 Å. Intermolecular H-bonds of the C–H···O type (Fig. S1, Table S4) link the molecules of **1** into layers parallel to the (100) plane. The crystal packing of **2** is realized without essential H-bonding (Fig. S2).

In the crystal packing of **3**, H-bonds of C–H···O and C–H···N types (Fig. S3, Table S12) link the molecules into

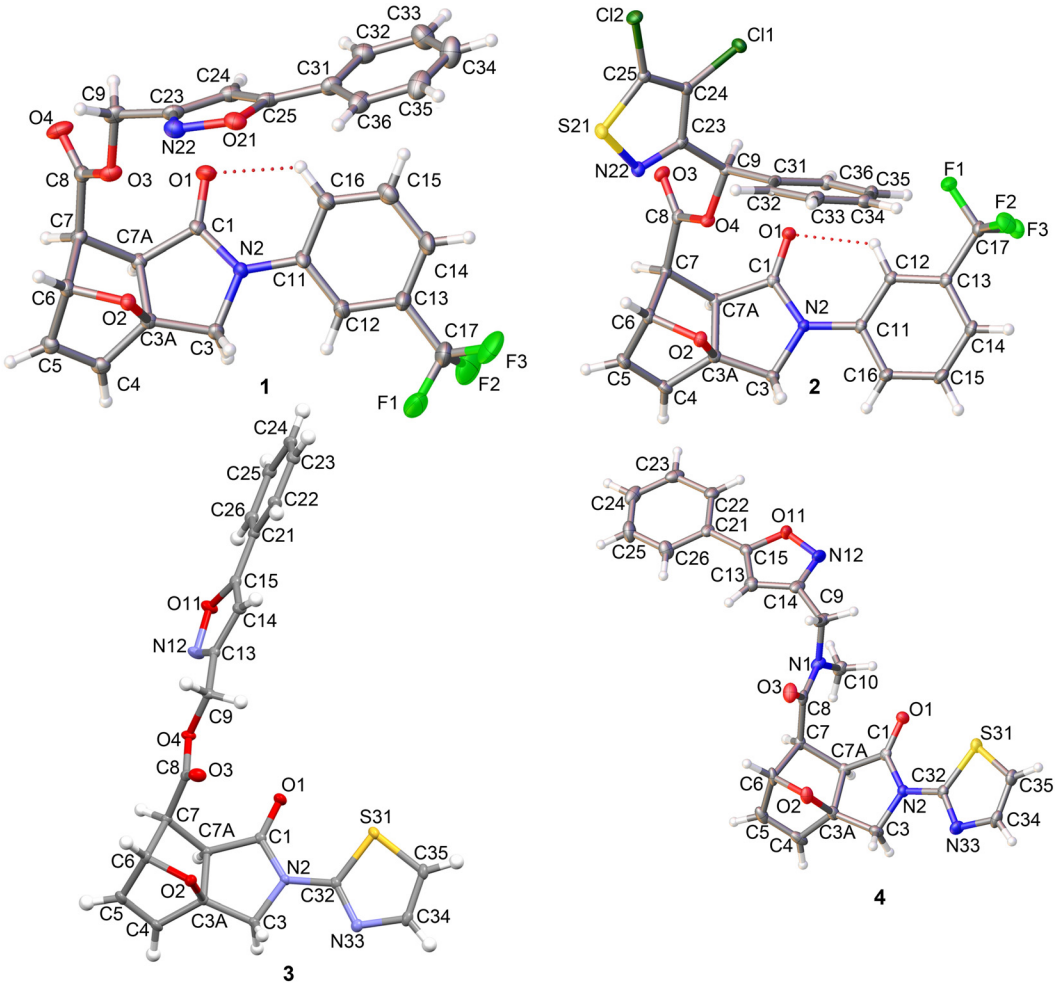

Fig. 1 Molecular structures of the molecules **1** (top left), **2** (top right), **3** (bottom left) and **4** (bottom right) showing atom numbering. Temperature displacement ellipsoids are drawn at the 50% probability level. Dotted line shows H-bonding interaction.

the chains along the [011] direction. In the structure **4**, H-bonds of C–H···O and C–H···S types (Fig. S4, Table S16) form layers parallel to the (001) plane.

DFT study

Initially, we optimized the solid-state geometries of compounds **1–4** using periodic boundary conditions (see Theoretical methods), and compared the computed structures with the corresponding experimental data (Fig. 2). A very good agreement was observed, with root-mean-square deviation (RMSD) values below 0.6 Å in all cases. The experimental and theoretical bond distances and angles relevant to the n → π* interactions and hydrogen/chalcogen bonding (HB/ChB) are summarized in Table 1.

Interestingly, the theoretical C···O distances are shorter and the O=C···O angles smaller in complexes **1–3** compared to **4**, suggesting that the C(ester)···O contacts are stronger than the C(amide)···O interactions. In compounds **3** and **4**, the S···O distances are shorter than the sum of the van der Waals radii (3.32 Å), consistent with the formation of chalcogen bonds. Since sulfur is known to be a weaker σ-hole donor than selenium or tellurium, the electrophilic role of sulfur in these two compounds is further analyzed in the following sections.

To investigate whether this molecular arrangement is an intrinsic property in the gas phase or a result of crystal packing effects, we also optimized isolated compounds **1–4**. The geometric data for these gas-phase structures are included in Table 1. A comparison reveals that the geometric features are in good agreement with the experimental data. Notably, the theoretical C···O distances are longer in the gas phase compared to the PBC calculations, suggesting that crystal packing favors the π-hole interactions. However, a direct comparison of the gas-phase distances with the experimental distances shows better agreement. The CH···O or S···O distances and angles also exhibit good agreement between the gas-phase and experimental values. The most significant difference is in the angle of the π-hole interaction, which shows more deviation for the gas-phase geometries in compounds **2** and **3**.

Table 1 Experimental (EXP), theoretical with periodic boundary conditions (PBC) and gas phase (GP) distances (Å) and angles (°) of the n → π* and HB/ChB interactions in compounds **1–4**

Compd.	C···O	O=C···O	O···H(S)	O···H(S)–C
1, PBC	2.862	95.7	2.228	116.6
1, GP	3.029	100.3	2.113	121.8
1, EXP	2.953	102.6	2.277	121.2
2, PBC	2.954	107.2	2.097	121.7
2, GP	3.145	120.9	2.108	121.8
2, EXP	3.017	109.6	2.170	124.3
3, PBC	3.013	101.6	2.827	159.2
3, GP	3.107	78.8	2.752	162.4
3, EXP	3.047	105.3	2.728	161.4
4, PBC	3.152	115.3	2.769	159.4
4, GP	3.102	113.9	2.755	162.3
4, EXP	3.068	110.7	2.791	161.6

To demonstrate the presence of n → π* and hydrogen/chalcogen bonding (HB/ChB) interactions, we employed NCIplot analysis and visualized the reduced density gradient (RDG) isosurfaces, which effectively depict noncovalent interactions in real space. The resulting plots are presented in Fig. 3, where, for clarity, only the n → π* (or π-hole···lone pair) and HB/ChB interactions are shown. Examination of these plots reveals that, for the ester derivatives **1–3**, the RDG

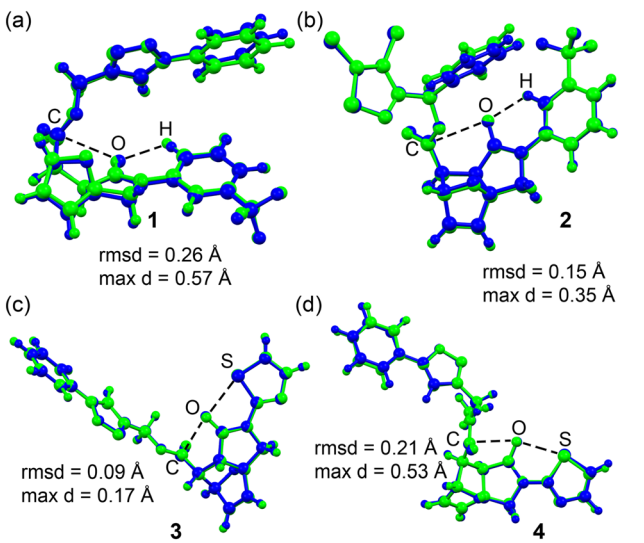

Fig. 2 Comparison of the experimental (in blue) and theoretical (in green) geometries of compounds **1** (a), **2** (b), **3** (c) and **4** (d). The RMSD and maximum displacement (max *d*) are also indicated.

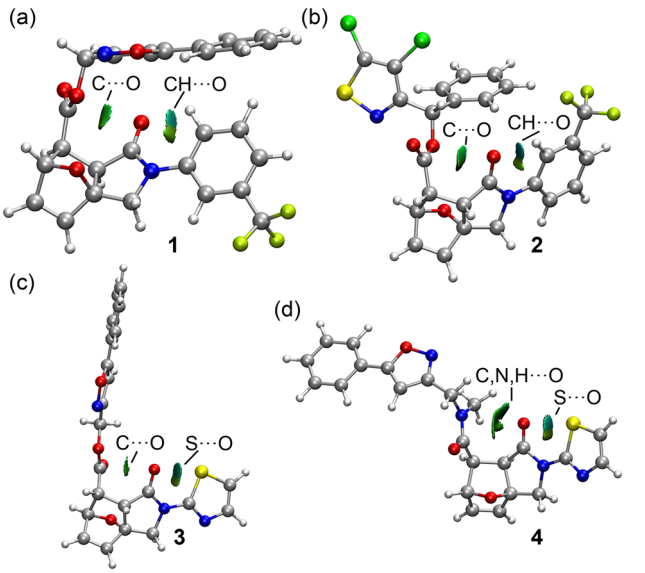

Fig. 3 NCIplot representation in compounds **1** (a), **2** (b), **3** (c), and **4** (d). Only the RDG isosurfaces characterizing C···O(oxo) and H, S···O(oxo) interactions are plotted. Settings: RDG = 0.45, ρ cut-off = 0.04 a.u., color range −0.04 a.u. ≤ (sign λ_2)ρ ≤ 0.04.

isosurfaces associated with the n → π* interactions are small and localized between the carbon and oxygen atoms, indicating a C···O contact. The RDG isosurface characterizing the C···O contact in compound **4** differs notably from those observed in compounds **1**–**3**. Specifically, the isosurface is larger and more diffuse, encompassing not only the carbon atom but also the nitrogen atom and the hydrogen atom of the methyl group attached to the amide nitrogen. This observation is consistent with the longer C···O distance and the wider O═C···O angle in compound **4**.

It is worth noting that quantum theory of atoms in molecules (QTAIM) analysis does not identify a bond critical point (BCP, where $\rho = 0$) or bond path between the carbon and oxygen atoms. Thus, this interaction is detectable only through the NCIplot method, which highlights regions where $\rho < 0.04$ a.u. This absence of a BCP and bond path in π-hole interactions has been discussed previously and is attributed to the low electron density at the π-hole donor atom.[35]

The NCIplot analysis also confirms the presence of CH···O hydrogen bonds in compounds **1** and **2**, and S···O chalcogen bonds (ChBs) in compounds **3** and **4**. Although this distinction is not immediately evident in Fig. 3, the RDG isosurfaces corresponding to the HB/ChB interactions display a bluish hue, while those representing the C···O contacts discussed earlier appear green, indicating that the latter are weaker, a conclusion consistent with previous studies.[7]

To further investigate these interactions, we conducted a natural bond orbital (NBO) analysis, which provides a detailed orbital-level understanding of donor–acceptor interactions. In particular, the second-order perturbation theory within the NBO framework quantifies the stabilization energies associated with each donor–acceptor charge transfer.

The results, summarized in Fig. 4, reveal that all four compounds exhibit the characteristic LP(O) → π*(C═O) charge transfer associated with n → π* interactions, with stabilization energies ranging from 0.6 kJ mol^{-1} in compound **4** to 2.6 kJ mol^{-1} in compound **1**. These values confirm that the n → π* interaction is weakest in compound **4**, consistent with its longer C···O distance. The observed stabilization energies are in good agreement with literature reports.[7]

The NBO analysis also reveals that the LP(O) → σ*(C–H) charge transfer interactions, corresponding to CH···O hydrogen bonds, are stronger than the n → π* interactions, reinforcing the conclusions drawn from the NCIplot analysis.

Remarkably, in compounds **3** and **4**, the NBO results further validate the chalcogen bond character of the S···O interactions, as evidenced by the LP(O) → σ*(C–S) charge transfer, which is characteristic of σ-hole interactions. The associated stabilization energies, 11.3 and 12.8 kJ mol^{-1} for compounds **3** and **4**, respectively, indicate that these ChBs are not only significantly stronger than the C···O contacts but also stronger than the CH···O hydrogen bonds, at least from an orbital interaction perspective.

Finally, to further support the existence of a σ-hole at the sulfur atom in the thiazole rings, we performed an electron localization function (ELF) analysis. This computational method is particularly effective for visualizing σ-holes and σ-lumps (lone pairs). The 2D ELF plots for compounds **3** and **4** are shown in Fig. 5. In both cases, the lone pair on the oxygen atom is clearly oriented toward the σ-hole on the sulfur atom, confirming the σ-hole character of the O···S contact.

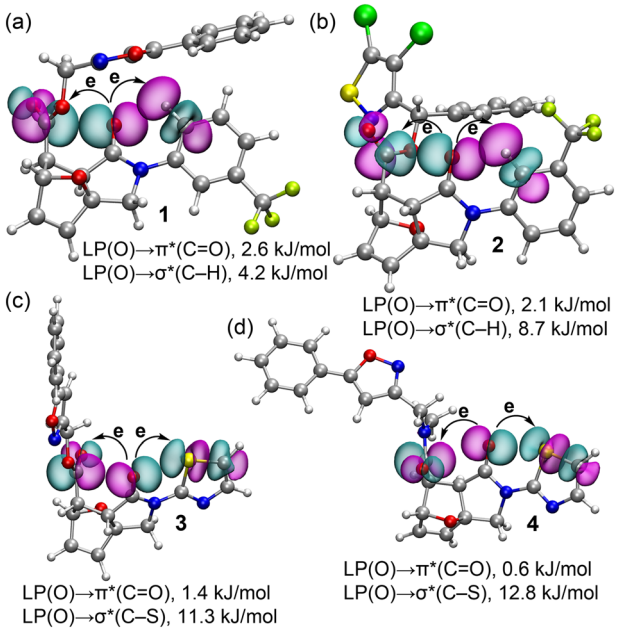

Fig. 4 NBOs corresponding to the LP(O) → π*(C═O) charge transfer in compounds **1** (a), **2** (b), **3** (c) and **4** (d). The NBOs corresponding to LP(O) → σ*(C–H) in **1** and **2** and LP(O) → σ*(C–S) charge transfer in **3** and **4** are also shown. The second order stabilization energies are also indicated.

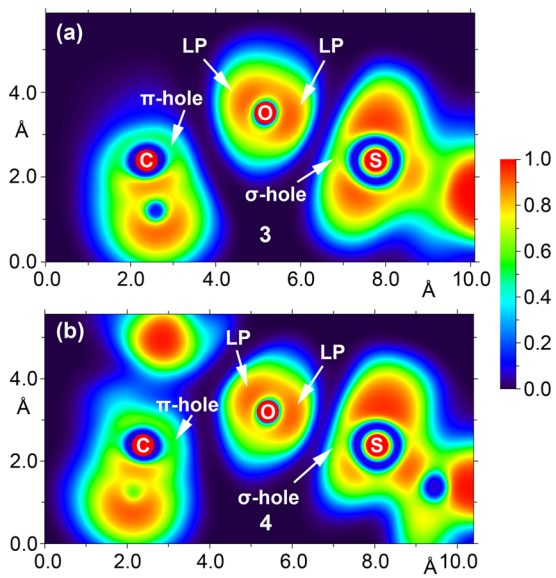

Fig. 5 2D ELF of compounds **3** (a) and **4** (b) in the plane defined by the three interacting atoms (C, O and S).

The ELF analysis also indicates that the directionality of the n → π* interaction is less favorable, with the oxygen lone pair only partially aligned toward the carbon atom. This observation aligns with the dominant chalcogen bond character inferred from the NBO analysis, further reinforcing the conclusion that the ChB interaction is stronger and more directional than the corresponding n → π* interaction in these systems.

Concluding remarks

In summary, we have synthesized and structurally characterized a series of azole-substituted 3*a*,6-epoxyisoindole-7-carboxylic acid derivatives, revealing how subtle structural variations influence noncovalent interaction patterns in the solid state. Through a combination of single-crystal X-ray diffraction and computational analyses (NCIplot, NBO, and ELF), we demonstrated that ester derivatives present stronger n → π* interactions than the amide analogue. Moreover, compound **2** containing an isothiazole ring and compound **3** containing a thiazole ring exhibit pronounced chalcogen bonding. The observed LP(O) → σ*(C–S) orbital interactions and the visualization of σ-holes *via* ELF maps confirm the role of sulfur atoms as effective σ-hole donors. These findings underscore the cooperative interplay of weak interactions in directing crystal packing and offer valuable insights for the design of supramolecular architectures in crystal engineering.

Author contributions

I. A. K. and V. I. P.: synthesis and spectral analysis, writing – original draft; V. P. Z. synthesis; R. M. G.: investigation and methodology; M. S. G. and E. V. N. X-ray experiments; A. F. and F. I. Z.: international collaboration, conceptualization, supervision, validation, project administration, writing – original draft, writing – review & editing.

Conflicts of interest

There are no conflicts to declare.

Data availability

All data supporting this article are provided in the SI. Crystallographic data for compounds **1**–**4** have been deposited with the Cambridge Crystallographic Data Centre (CCDC) under accession numbers 2413571–2413574. These files are also included in the supplementary materials. See DOI: **https://doi.org/10.1039/D5CE00673B**.

CCDC 2413571–2413574 contain the supplementary crystallographic data for this paper.[36]

Acknowledgements

This publication has been supported by the Russian Scientific Foundation (project number 23-43-10024) (FIZ) and the Belarusian Republican Foundation for Fundamental Research (project number X23RNF-051) (VIP). We thank the MICIU/AEI from Spain for financial support (project number PID2020-115637GB-I00, FEDER funds). X-ray diffraction experiments were performed at the Center for Shared Use of Physical Methods of Investigation at the Frumkin Institute of Physical Chemistry and Electrochemistry, RAS.

Notes and references

1 (*a*) G. L. Petri, M. V. Raimondi, V. Spanò, R. Holl, P. Barraja and A. Montalbano, *Top. Curr. Chem.*, 2021, **379**, 34; (*b*) S. Poyraz, H. A. Döndaş, N. Y. Döndaş and J. M. Sansano, *Mini-Rev. Med. Chem.*, 2023, **14**, 1239658.

2 (*a*) F. Omar, A. M. Tareq, A. M. Alqahtani, K. Dhama, M. A. Sayeed, T. B. Emran and J. Simal-Gandara, *Molecules*, 2021, **26**, 2297; (*b*) T. P. Singh and O. M. Singh, *Mini-Rev. Med. Chem.*, 2018, **18**, 9–25; (*c*) M.-L. Luo, W. Huang, H.-P. Zhu, C. Peng, Q. Zhao and B. Han, *Biomed. Pharmacother.*, 2022, **149**, 112827; (*d*) L. Luo and K. Keyomarsi, *Expert Opin. Invest. Drugs*, 2022, **25**, 1354–3784.

3 J. Zhu, J. Mo, H.-Z. Lin, Y. Chen and H.-P. Sun, *Bioorg. Med. Chem.*, 2018, **26**, 3065–3075.

4 A. V. Kletskov, N. A. Bumagin, F. I. Zubkov, D. G. Grudinin and V. I. Potkin, *Synthesis*, 2020, 159–188.

5 (*a*) V. A. Kulchitsky, V. I. Potkin, Y. S. Zubenko, A. N. Chernov, M. V. Talabaev, Y. E. Demidchik, S. K. Petkevich, V. V. Kazbanov, T. A. Gurinovich, M. O. Roeva, D. G. Grigoriev, A. V. Kletskov and V. N. Kalunov, *Med. Chem.*, 2012, **8**, 22–32; (*b*) V. Kulchitsky, A. Zamaro, V. Potkin, K. Suziedelis, S. Koulchitsky and Z. Kaliadzich, *J. Cancer Sci. Ther.*, 2019, **2**, 119–120.

6 G. R. Desiraju, *J. Am. Chem. Soc.*, 2013, **135**, 9952–9967.

7 (*a*) R. W. Newberry, B. VanVeller, I. A. Guzei and R. T. Raines, *J. Am. Chem. Soc.*, 2013, **135**, 7843–7846; (*b*) R. W. Newberry and R. T. Raines, *Acc. Chem. Res.*, 2017, **50**, 1838–1846; (*c*) M. Egli and S. Sarkhel, *Acc. Chem. Res.*, 2007, **40**, 197–205.

8 (*a*) H. B. Bürgi, J. D. Dunitz and E. Shefter, *J. Am. Chem. Soc.*, 1973, **95**, 5065–5067; (*b*) H. B. Bürgi, J. D. Dunitz, J. M. Lehn and G. Wipff, *Tetrahedron*, 1974, **30**, 1563–1572; (*c*) H. B. Bürgi and J. D. Dunitz, *Acc. Chem. Res.*, 1983, **16**, 153–161.

9 (*a*) I. Caracelli, J. Zukerman-Schpector, I. Haiduc and E. R. T. Tiekink, *CrystEngComm*, 2016, **18**, 6960–6978; (*b*) I. Caracelli, J. Zukerman-Schpector and E. R. T. Tiekink, *Coord. Chem. Rev.*, 2012, **256**, 412–438; (*c*) A. Das, S. R. Choudhury, C. Estarellas, B. Dey, A. Frontera, J. Hemming, M. Helliwell, P. Gamez and S. Mukhopadhyay, *CrystEngComm*, 2011, **13**, 4519–4527; (*d*) Z. Lu, P. Gamez, I. Mutikainen, U. Turpeinen and J. Reedijk, *Cryst. Growth Des.*, 2007, **7**, 1669–1671; (*e*) N. P. Funnell, C. L. Bull, C. J. Ridley, S. Parsons and J. P. Tellam, *Chem. Commun.*, 2020, **56**, 6428–6431; (*f*) A. Bauza, A. Frontera and T. J. Mooibroek, *Cryst. Growth Des.*, 2016, **16**, 5520–5524.

10 (*a*) R. W. Newberry and R. T. Raines, *ACS Chem. Biol.*, 2014, **9**, 880–883; (*b*) R. W. Newberry and R. T. Raines, *Acta Crystallogr., Sect. E: Crystallogr. Commun.*, 2016, **72**, 136–139.

11 (*a*) A. Choudhary, K. J. Kamer and R. T. Raines, *J. Org. Chem.*, 2011, **76**, 7933–7937; (*b*) C. Cabezas, J. L. Alonso, J. C. López and S. Mata, *Angew. Chem., Int. Ed.*, 2012, **51**, 1375–1378.
12 F. E. Hanna, A. D. Bond and C. A. Hunter, *Chem. Sci.*, 2025, **16**, 7894–7901.
13 S. Munawar, A. F. Zahoor, S. M. Hussain, S. Ahmadd, A. Mansha, B. Parveen and K. G. Ali, *Heliyon*, 2024, **10**, e23416.
14 A. V. Varlamov, E. V. Boltukhina, F. I. Zubkov, N. V. Sidorenko, A. I. Chernyshev and D. G. Grudinin, *Chem. Heterocycl. Compd.*, 2004, **40**, 22–28 (*Khim. Geterotsikl. Soedin.*, 2004, 27–33).
15 V. I. Potkin, S. K. Petkevich, A. V. Kletskov, E. A. Dikusar, Yu. S. Zubenko, N. A. Zhukovskaya, V. V. Kazbanov and S. G. Pashkevich, *Russ. J. Org. Chem.*, 2013, **49**, 1523–1533.
16 V. I. Potkin, N. A. Bumagin, A. V. Kletskov, S. K. Petkevich and P. V. Kurman, *Russ. J. Org. Chem.*, 2016, **52**, 1661–1669.
17 E. A. Akishina, E. A. Dikusar, S. K. Petkevich, R. S. Alexeyev, N. A. Bumagin and V. I. Potkin, *Russ. J. Gen. Chem.*, 2021, **91**, 1512–1518.
18 D. Marx, G. Schnakenburg, S. Grimme and C. E. Müller, *Molecules*, 2019, **24**, 2168.
19 *SAINT-Plus (Version 8.40B)*, Bruker AXS Inc., Madison, Wisconsin, USA, 2019.
20 L. Krause, R. Herbst-Irmer, G. M. Sheldrick and D. Stalke, *J. Appl. Crystallogr.*, 2015, **48**, 3–10.
21 G. M. Sheldrick, *Acta Crystallogr., Sect. A: Found. Adv.*, 2015, **71**, 3–8.
22 G. M. Sheldrick, *Acta Crystallogr., Sect. C: Struct. Chem.*, 2015, **71**, 3–8.
23 A. D. Becke, *Phys. Rev. A: At., Mol., Opt. Phys.*, 1988, **38**, 3098–3100.
24 J. P. Perdew, *Phys. Rev. B: Condens. Matter Mater. Phys.*, 1986, **33**, 8822–8824.
25 D. V. Oliveira, J. Laun, M. F. Peintinger and T. Bredow, *J. Comput. Chem.*, 2019, **40**, 2364–2376.
26 S. Eichkorn, F. Weigend, O. Treutler and R. Ahlrichs, *Theor. Chem. Acc.*, 1997, **97**, 119–124.
27 (*a*) S. Grimme, J. Antony, S. Ehrlich and H. Krieg, *J. Chem. Phys.*, 2010, **132**, 154104; (*b*) S. Grimme, S. Ehrlich and L. Goerigk, *J. Comput. Chem.*, 2011, **32**, 1456–1465.
28 C. Adamo and V. Barone, *J. Chem. Phys.*, 1999, **110**, 6158–6170.
29 F. Weigend and R. Ahlrichs, *Phys. Chem. Chem. Phys.*, 2005, **7**, 3297–3305.
30 T. Lu and F. Chen, *J. Comput. Chem.*, 2012, **33**, 580–592.
31 W. Humphrey, A. Dalke and K. Schulten, *J. Mol. Graphics*, 1996, **14**, 33–38.
32 E. D. Glendening, J. K. Badenhoop, A. E. Reed, J. E. Carpenter, J. A. Bohmann, C. M. Morales and F. Weinhold, *NBO 7.0*, Theoretical Chemistry Institute, University of Wisconsin, Madison, 2018.
33 A. D. Becke and K. E. Edgecombe, *J. Chem. Phys.*, 1990, **92**, 5397–5403.
34 A. Jordan, K. D. Whymark, J. Sydenham and H. F. Sneddon, *Green Chem.*, 2021, **23**, 6405.
35 E. C. Escudero-Adán, A. Bauzá, C. Lecomte, A. Frontera and P. Ballester, *Phys. Chem. Chem. Phys.*, 2018, **20**, 24192–24200.
36 (*a*) I. A. Kolesnik, V. I. Potkin, M. S. Grigoriev, R. M. Gomila, E. V. Nikitina, V. P. Zaytsev, F. I. Zubkov and A. Frontera, CCDC 2413571: Experimental Crystal Structure Determination, 2025, DOI: **10.5517/ccdc.csd.cc2m0j4b**; (*b*) I. A. Kolesnik, V. I. Potkin, M. S. Grigoriev, R. M. Gomila, E. V. Nikitina, V. P. Zaytsev, F. I. Zubkov and A. Frontera, CCDC 2413572: Experimental Crystal Structure Determination, 2025, DOI: **10.5517/ccdc.csd.cc2m0j5c**; (*c*) I. A. Kolesnik, V. I. Potkin, M. S. Grigoriev, R. M. Gomila, E. V. Nikitina, V. P. Zaytsev, F. I. Zubkov and A. Frontera, CCDC 2413573: Experimental Crystal Structure Determination, 2025, DOI: **10.5517/ccdc.csd.cc2m0j6d**; (*d*) I. A. Kolesnik, V. I. Potkin, M. S. Grigoriev, R. M. Gomila, E. V. Nikitina, V. P. Zaytsev, F. I. Zubkov and A. Frontera, CCDC 2413574: Experimental Crystal Structure Determination, 2025, DOI: **10.5517/ccdc.csd.cc2m0j7f**.